Royal Norwegian Council
for Scientific and Industrial Research
(NTNF)

NORSAR

NORSAR Scientific Report No. 2-92/93

Semiannual Technical Summary

1 October 1992 — 31 March 1993

Kjeller, July 1993

APPROVED FOR PUBLIC RELEASE, DISTRIBUTION UNLIMITED

7.2 Intelligent post-processing of seismic events -- Part 2: Accurate determination of phase arrival times using autoregessive likelihood estimation

Introduction

A precise estimation of the onset time of seismic phases is necessary to obtain an accurate event location. In the context of automatic processing of the regional arrays operated by NORSAR, a two-step procedure has been in use since the first regional array, NORESS, was established in 1985 (Mykkeltveit and Bungum, 1984). This procedure consist of first applying a series of STA/LTA detectors in parallel to a set of filtered beams. When one or more of the STA/LTA detectors exceed a predefined threshold, a phase detection is declared and a detection time is found. Subsequently, a time domain phase timing algorithm is applied to the filtered beam with the highest SNR, using the detection time as the starting value. A detailed description of this algorithm is found in Mykkeltveit and Bungum (1984).

These estimates of the onset times are used by the automatic phase association and event location procedure (ESAL) of the Intelligent Monitoring System (IMS) (Bache et al, 1993), and the fully automatic processing results are finally reviewed and corrected by the analyst using the Analyst Review Station (ARS) of the IMS. Through the analyst review we have experienced that in most cases the phase onsets need to be adjusted. In section 7.6 of this report, comparisons between the automatic and manual onset time estimates of various seismic phases are presented. For P-type phases the standard deviations of automatic - manual onset time generally varies between 0.5 and 0.7 seconds. It should be noticed that these estimates represent averages for all seismic phases for a one-week period, and thus include phases with very different SNR's, frequency characteristics and signatures. For phases with an high SNR and an instantaneous signature, the performance of the phase timing algorithm is significantly better. Nevertheless, one of the conclusions from the study presented in section 7.6 is that in order to improve the precision of the automatic event locations provided by the IMS and in order to reduce the analyst's workload, there is a strong need to improve the precision of the automatic onset time estimates.

In this study we will investigate the potential automatic use of an onset picker based on autoregressive likelihood estimation (Pisarenko et al, 1987, Kushnir et al, 1990). Both a single-component version (ESTON1) and a three-component version (ESTON3) of this method will be tested on data from events located in the Khibiny Massif on the Kola Peninsula of Russia, recorded at the Apatity array, the Apatity three-component station and the ARCESS array, see Fig. 7.2.1.

The Khibiny Massif events

Six apatite mines are located within an area of about 10 km^2 in the Khibiny Massif (see Fig. 7.2.1).A detailed description of these mines and the mining activity is found in Mykkeltveit (1992). The coordinates of the mines are given in Table 7.2.1. Notice that Mine I consists of both an underground mine and an open-pit mine. Although we have no explicit information on the exact sizes of these mines, interpretation of various maps suggest that the typical size is about 1 km^2. The Kola Regional Seismological Centre has since the beginning of 1991 provided NORSAR with information on mining blasts in the six Khibiny mines. The information provided contains an assignment of the relevant mine (I-VI), P (and normally also S) arrival times at the analog APA (Apatity) station (co-located with the three-component station), the amplitude and period of the signal, and the total charge size in tons. Detailed information on the 58 events used in this study is given in Table 7.2.2.

At the Apatity array (APA0) and the Apatity three-component station (APZ9) which are located within a distance range of 18 - 49 km from the different Khibiny mines, the seismograms show clear P (Pg), S (Sg or Lg) and Rg arrivals (see Figs. 7.2.2 and 7.2.3). At ARCESS which is located about 400 km from the mines, a clear Pn and emergent Pg, Sn and Lg phases are observed (see Fig. 7.2.4). Table 7.2.3 gives detailed information on the distances and azimuths from APZ9, APA0 and ARCESS to the six Khibiny mines.

Estimation of P arrival time

We will not go into any detail concerning the theory of the autoregressive likelihood technique for onset time estimation, but refer to Pisarenko et al (1987) and Kushnir et al (1990) for details. We will, however, concentrate on the practical aspects of implementing the method as part of an automatic processing sequence. The onset time procedure requires that we have available an approximate timing of the phase arrival, and the search for the exact onset is limited to an interval around the initial arrival time. The initial arrival time can be obtained in several ways:

- Pisarenko et al (1987) and Kushnir et al (1990) suggest that an optimal event detector based on an Bayesian approach using autoregressive modelling of the data should be used for phase detection and approximate timing.
- Another alternative, which we will use for P-phases at APA0 and ARCESS, is to take the onset time provided by the IMS as the initial estimate. This onset time is calculated using the algorithm described in the *Introduction.*
- A third alternative is to use the predicted phase arrival time, e.g., derived from an initial event location and origin time or from the expected pattern of phase arrivals from events in a given region. This is the approach to be used for both P- and S-phases at APZ9 and for S-phases at APA0.

The autoregressive likelihood estimator is based on regarding the signal onset time as the moment in time when the statistical features of the observed time series (single-component or three-component) are abruptly changed. The single-component method thus takes into account changes in both power and frequency content, and it is therefore important that the broadband signal waveforms are retained (no narrow bandpass filtering). In addition to taking into account changes in power and frequency content, the three-component method is also sensitive to changes in the polarization characteristics of the three-component data. From experimenting with both ESTON1 and ESTON3 we have found that in order to obtain stable estimates, the data should first be lowpass filtered and decimated according to the highest frequencies of the signals. For P-phases from the Khibiny events recorded at the Apatity stations and at ARCESS, signal frequencies up to the Nyquist frequency of 20 Hz are in almost all cases observed. Consequently, no lowpass filtering or decimation is applied to the data. However, a low-order prediction error filter, designed from a 25 second noise sample preceding the P-phase, is applied.

For the arrays APA0 and ARCESS, the slowness and azimuth of the P-phases are computed using broad-band f-k analysis (Kværna and Doornbos, 1986). Kværna and Ringdal (1986) showed that the key to obtain stable slowness and azimuth estimates of phases from a given region is to process the data in a fixed frequency band, using a fixed time window positioning. The time window positioning for the f-k analysis and the fact that the onset time is computed from a steered beam (with steering delays found from f-k analysis) make these two processes to be closely integrated. Through extensive testing we have found that for P-phases from the Khibiny mines recorded at APA0, the most stable slowness and azimuth estimates are obtained if the f-k spectrum is computed in the frequency band 4.0 - 10.0 Hz using the 9 SPZ-component sensors of the array. The time window has a length of 2 seconds and starts 0.3 seconds ahead of the P-arrival. For ARCESS the most stable estimates are obtained if all 25 SPZ-component sensors are processed in the frequency band 3.0 - 6.0 Hz using a 3 second time window starting 0.3 seconds ahead of the P-arrival. Further refinement can be made by including a procedure that checks the SNR in the predefined frequency band, and adjusts the frequency cutoffs in the case of low SNR.

For APA0 and ARCESS, the automatic algorithm used for estimating the P-onsets from events from the Khibiny Massif can be summarized in the following way:

- Use the P onset from the IMS as the initial arrival time estimate.
- Generate a beam with steering delays corresponding to the IMS f-k results and prewhiten the beam with a low order prediction error filter.
- Apply ESTON1 to the prewhitened beam in an interval of ±2 seconds around the initial onset estimate. A sliding window length of 1 second is used by ESTON1, and the autoregressive modelling is of order 3.
- Position the time window according to the onset time from ESTON1 and run the f-k analysis as outlined above.
- Generate a new beam with steering delays corresponding to the new f-k results and prewhiten the beam with a low order prediction error filter.
- Apply ESTON1 to the new prewhitened beam in an interval of ±2 seconds around the previous ESTON1 onset estimate.
- Position the time window according to the last onset time estimate from ESTON1 and run the f-k analysis once more as outlined above.

For the three-component station APZ9 the situation is somewhat different as this station is not part of the automatic IMS processing. APZ9 is, however, located only 18 km from APA0, and we therefore choose to use the onset time at APA0 as the initial arrival time estimate. The processing can be summarized as follows:

- Use the P onset at APA0 as the initial arrival time estimate.

- Prewhiten the Z-component APZ9 with a low order prediction error filter.
- Apply ESTON1 to the prewhitened Z-component APZ9 in an interval of ±5 seconds around the initial onset estimate from APA0. The sliding window length used by ESTON1 is 1 second and the autoregressive modelling is of order 3.
- Reestimate the onset time applying ESTON1 to the prewhitened z-component APZ9 in an interval of ±2seconds around the previous ESTON1 onset estimate.

Precision of automatic P-onsets using the single-component estimator (ESTON1)

The precision of the automatic P-onsets using ESTON1 has been assessed by two different methods. The first method is to compare the ESTON1 estimates to the best manual pick. The purpose of this approach is to obtain information on any bias in ESTON1 estimates, and also to check the consistency between the automatic and manual onset estimates. In the second method we estimate the standard deviation of the phase picks by looking at the consistency of the arrival time differences between phases from events located in the same mine, see Sereno (1990). In this way, an unbiased estimate of the standard deviation is found for both the automatic and manual picks.

In Fig. 7.2.5.a the time differences between the automatic onsets from IMS and the manual pick at APA0 are presented as a function of signal-to-noise ratio (SNR) on the prewhitened beam. The standard deviation of these differences is as high as 0.43 seconds. In comparison, the time difference between the automatic ESTON1 onsets and the manually picked onsets, given in Fig. 7.2.5.b has a standard deviation as low as 0.02 seconds, and has a systematic positive bias of 0.05 seconds, i.e. the ESTON1 onsets are consistently picked a bit late.

In Fig. 7.2.6 similar plots are presented for Pn phases recorded at ARCESS. The automatic onsets from IMS shows significantly less scatter ($\sigma = 0.13$ s) than for APA0. On the other hand, the automatic ESTON1 onsets has a somewhat larger scatter ($\sigma = 0.03$ s) and a somewhat larger positive bias (0.08 s) than at APA0. Nevertheless, the accuracy of the ESTON1 time picks appears to be significantly better than those of the current processing system.

To address possible dependency of ESTON1 on the signal-to-noise ratio, we have in Fig. 7.2.7 plotted the time difference between the automatic ESTON1 onsets and the manually picked onsets for both APA0 and APZ9. In this way, we get an overview of the scatter for SNR's ranging from about 3 to about 500. We find from this figure that the time differences seem to be almost independent of SNR, which again indicate that the ESTON1 onset estimator works well for quite low signal-to-noise ratios. For direct comparison, we have in Fig. 7.2.8 plotted the ARCESS data on the same scale, but for ARCESS no low SNR phases are observed, as all SNR's exceed 6. By SNR, we mean the maximum of the linear ratio STA/LTA (i.e., short term average divided by long term average.)

The results presented above show that an automatic onset time procedure for P-phases using ESTON1 can give a remarkable improvement in precision compared to the current algorithm used in the IMS. The ESTON1 onset estimator has a bias that is dependent on the dominant frequency of the signal. At the Apatity stations the average dominant P frequency is 13 Hz and the average bias is 0.05 s, whereas at ARCESS the average dominant P frequency is 6 Hz and the average bias is 0.08 s. The difference in bias can not be due to differences in sampling rate, since both APA0, APZ9 and ARCESS have a sampling frequency of 40 Hz. For the high frequency signals at the Apatity stations, the bias shows no clear dependency on SNR, at least not for SNR above 3. As expected, the results also suggest that the precision of ESTON1 increases with increasing signal frequencies. This can be inferred from the fact that the automatic P-onset estimates of the high-frequency signals at the Apatity stations are more consistent with the manual picks than the P-onsets at ARCESS, which generally have a lower dominant frequency. According to Pisarenko et al (1987) there are no analytical expressions for the theoretical biases and variances of ESTON1 and ESTON3, and it is therefore necessary to obtain empirical values. In any case, the biases and variances are less than 0.1 s for the P-phases considered in this study.

An unbiased estimate of the measurement variance is determined from the arrival time difference between two phase observations for repeated events in the same mine. Specifically:

$$\sigma^2_{1,pick} + \sigma^2_{2,pick} = \frac{\sum_{k=1}^{N_{mines}} \sum_{i=1}^{N_{obs}} [\Delta T_{obs_{ik}} - \langle \Delta T_{obs} \rangle_k]^2}{(N_{obs} - N_{mines})}$$

where σ_1^2 and σ_2^2 are the picking variances of each phase, $\Delta T_{obs_{ik}}$ is the *ith* observation of the arrival-time difference for the *kth* mine. $\langle \Delta T_{obs} \rangle_k$ is the mean arrival time difference for the *kth* mine. N_{obs} is the total number of observations (at all mines), and N_{mines} is the number of mines.

By computing the arrival-time differences between the P observations at the three stations APA0(1), APZ9(2) and ARCESS(3), we get three equations of the type above, with altogether three unknowns. These equations can easily be solved to obtain estimates of each individual variance value. For example, for the automatic picks we obtain:

$$\sigma_1^2 + \sigma_2^2 = (0.065)^2$$

$$\sigma_1^2 + \sigma_3^2 = (0.065)^2$$

$$\sigma_2^2 + \sigma_3^2 = (0.074)^2$$

which gives $\sigma_1 = 0.04$, $\sigma_2 = 0.05$ and $\sigma_3 = 0.05$ (see Table 7.2.4).

The standard deviations of both the manual picks and the automatic picks from ESTON1 are given in Table 7.2.4. All standard deviations are less than or equal to 0.06 s, and a part of this variability is likely due to the fact that the events of each mine are not located at the same spot, but are distributed within the mine. Under the assumption that each mine has an extent of 1 x 1 km (which is reasonable from interpretation from various maps), we have computed the maximum theoretical P travel-time difference between APA0 and APZ9 for the six Khibiny mines. The largest value is obtained for Mine I, where a 0.09 s travel-time difference is possible. The smallest values are found for Mine V and Mine VI, where a 0.04 s travel-time difference is possible. This clearly suggest that location variability within each mine can have a significant impact on the estimates of the picking precision. If we, however, assume that the distribution of the events within each mine increases all picking error estimates with a similar amount, a likely interpretation of the differences in picking precision between the three stations is as follows:

- The P picks at APZ9 are less precise than at APA0 due to generally lower SNR.
- The P picks at ARCESS are less precise than at APA0 due to generally lower dominant frequency of the signals.

The results of Table 7.2.4 show that the automatic ESTON1 method matches the human precision, and that for the relatively high SNR P arrivals analyzed in this study, the standard deviation of the automatic picks is well below 0.1 s.

Estimation of S arrival time at the Apatity stations

As seen from Fig. 7.2.2 and 7.2.3, the seismograms of the Khibiny events show clear P, S and Rg arrivals at the Apatity stations APA0 and APZ9. The S-onsets do, however, become more emergent with increasing source-receiver distance. The S-phases typically have the largest SNR on the transverse component, but they are also clearly observed on the radial and vertical components. For automatic estimation of S-onsets, we have experimented with both the single-component ESTON1 onset estimator applied to the transverse component, and the three-component ESTON3 onset estimator applied to the three-component data, and found that the ESTON3 method gave the best results. The most stable results were obtained if the data were first filtered in a relatively wide band between 2.0 and 8.0 Hz and then decimated to a sampling rate of 20 Hz.

The Rg arrivals occur very close in time to the S-onset. Moreover, the Rg phase is dispersive. We therefore did not succeed in estimating the Rg-onset in a reliable way with the autoregressive likelihood estimation technique. In order to design an automatic processing sequence for the Khibiny events at the Apatity stations APA0 and APZ9, we have utilized the expected pattern of phase observations from events in this region, and the procedure is as follows:

- Estimate P-onset as previously outlined
- Identify the peak of the Rg-phase from an STA envelope created from the filtered z-component (0.8 - 2.0 Hz). The search interval for the Rg maximum is currently limited to 20 seconds after the P-onset.

- For the APA0 array, the slowness and azimuth of the Rg phase is estimated using data in a 5 s window starting 3 s ahead of the Rg peak. A frequency band of 0.8 - 2.0 Hz is used in the f-k analysis.
- For estimation of S-onsets, the three-component data are first filtered and decimated as outlined above, and the ESTON3 estimator is then applied within a time interval that starts 2 s after the P-onset and stops at the time of the Rg peak. The sliding window length used by ESTON3 is 2 seconds and the autoregressive modelling is of order 3.
- For the APA0 array, the slowness and azimuth of the S phase is estimated using data in a 2 s window starting 0.3 s ahead of the S-onset. A frequency band of 2- 5 Hz is used in the f-k analysis.

Illustrations of the automatic processing sequence are shown if Figs. 7.2.9 and 7.2.10. Notice the clear peak of the ESTON3 likelihood function at the S-onset for both events.

Precision of automatic S-onsets using the three-component estimator (ESTON3)

When comparing the automatic ESTON3 onsets to the manually picked S-onsets at APA0, we find that the standard deviation of the time differences is 0.18 s and that the bias is 0.01 s. For APZ9 the standard deviation is 0.12 s and the bias is 0.04 s. Due to the relatively large scatter in the observations, this bias of 0.04 is not significantly different from 0.

To compute the measurement variance of the S-onset estimates, we have again investigated the consistency of the arrival time difference between two phase observations for repeated events in the same mine, according to equation 7.2.1. By using the P-onsets at both APA0, APZ9 and ARCESS as references, for which the measurement variances are known (see. Table 7.2.4), we can reliably estimate both the manual and the automatic S-onset variances at both APA0 and APZ9. The results are summarized in Table 7.4.5

We see from Table 7.4.5 that the picking uncertainty estimates based on all three reference P-phases are very consistent, indicating that the method for estimating uncertainty works well. The fact that the precision of the manual and automatic picks are about equal, indicates that the automatic S-onset algorithm using ESTON3 matches the human precision. Table 7.4.5 also show that the S-onsets at APZ9 ($\sigma = 0.13$ s) are generally more precise than at APA0 ($\sigma = 0.19$ s). We believe that this is due to the fact that the S-phases become more emergent with increasing source-receiver distance, as illustrated in Figs. 7.2.2 and 7.2.3. The six Khibiny mines are located within a distance range of 18 - 33 km from APZ9, and within a distance range of 32 - 49 km from APA0, see Table 7.2.3.

It would have been interesting to compare the precision of the automatic S-onsets from ESTON3 to the precision of the automatic S-onsets used by the IMS. We have, however, experienced that the continuous processing of the Apatity array data (APA0) has problems in detecting and estimating the onsets, slowness and azimuths of secondary phases that have little time separation and large differences in frequency content. The first S-detection of the Khibiny events recorded at APA0 is in almost all cases declared in a low frequency band, which is typical for detection of Rg. Consequently the onset routine prefilters the data in a low passband, e.g. 1 - 2 Hz, where S has a low SNR, and the first S-onset is in many cases missed. With this problem in mind we have found it difficult to justify a comparison between the automatic S-onsets from ESTON3 and the automatic S-onsets from the procedure providing data to the IMS.

Precision of azimuth estimates from broad-band f-k analysis

As described above, the estimation of onset time and the estimation of slowness and azimuth by f-k analysis are closely integrated processes. In one-array location of seismic events, the azimuth estimates are necessary to be able to compute an event location, and in the event location procedure of the IMS (Bratt and Bache, 1988) the phase azimuth estimates are required to be accompanied with an uncertainty estimate.

In Table 7.5.6, the mean and the standard deviation of the azimuth residuals relative to the Khibiny mine locations of the phases recorded at the arrays APA0 and ARCESS are presented. We see from the table that the P and Rg azimuths at APA0 have about the same standard deviation (3.9 and 3.4 degrees, respectively), but that the P azimuths have a systematic bias of 8.2 degrees. The Rg azimuth bias is as low as -1.8 degrees. The ARCESS P azimuths have a very low standard deviation (0.9 degrees), but a systematic bias of 4.6 is consistently observed. The S-azimuths at APA0 show a very large scatter. This show that if the Khibiny events are located without introducing corrections for the azimuth biases, the Rg azimuths should be given the smallest a priori uncertainty. If the systematic biases are removed, the a priori uncertainty of P and Rg at APA0 become comparable. With the systematic bias removed, the a priori uncertainty of ARCESS P is very small, but it should be noticed that in the event location procedure (Bratt and Bache, 1988) the a priori azimuth uncertainty is scaled by the source-receiver distance, such that an azimuth observation at 400 km distance with an uncertainty of 0.9 degrees (ARCESS P) is given less weight than an azimuth observation at 40 km distance with an uncertainty of 3.9 degrees (APA0 P).

Conclusions

The results presented in this study show that very precise automatic estimates of phase onsets from events in the Khibiny Massif can be obtained with the autoregressive likelihood estimation method. Implementation of the method requires that we have available approximate estimates of the phase arrival, and we have shown that such approximate estimates can be obtained from the IMS event definitions (phase association and event location) or from analysis of previous events in the region. In this way, the autoregressive likelihood estimation method can provide phase onsets that match the human precision. The uncertainties and biases of the automatic onset estimates of various phases at the Apatity stations and at ARCESS have been quantified, and the precision of the automatic phase picks shows very large improvement in comparison to the automatic phase onsets from the continuous processing providing input to the IMS.

In addition to the automatic onset estimation, we have estimated the phase azimuths and slowness using broad-band f-k analysis. This has been done using data in a fixed frequency band, using a fixed window positioning, as suggested by Kværna and Ringdal

(1986) for the purpose of obtaining increased stability. For P-phases recorded at ARCESS, the results are in accordance with those of Kværna and Ringdal (1986), where a scatter of only ±1 degree were observed at NORESS for Pn phases from repeated events at a distance of 300 km. Comparing to the overall azimuth uncertainty of phases recorded at ARCESS and NORESS (Sereno, 1990), we find that if the systematic biases are removed from our azimuth estimates, the event location precision can be significantly improved. Without introducing azimuth corrections, the Rg azimuths at APA0 show to be quite reliable.

We realize that in order to obtain accurate event locations, precise onset time and azimuth estimates are necessary, but not sufficient. If the theoretical travel-time model used in the event location deviates from the true travel-times, the precision of the event locations will be reduced. To overcome this, we will in Section 7.3 of this report discuss the introduction of travel-time corrections.

A natural extension to this study will be to investigate the performance of ESTON1 and ESTON3 applied to phases at the other stations of the network recording the Khibiny events. At NORESS and FINESA the detected Pn phases have quite low SNR, and it would be interesting to quantify the precision of the automatic onset estimates of these phases. It also remains to test and implement the automatic picking of Sn and Lg phases at ARCESS, NORESS and FINESA.

During the work with the autoregressive likelihood estimation method, we have experienced that the display of the likelihood functions, as illustrated in Figs. 7.2.9 and 7.2.10 can assist the analyst in picking correct phase onsets. In the context of interactive analysis of seismic data, we believe that the idea of making such likelihood functions available to the analyst should be pursued.

T. Kværna

References

Bache, T.C., S.R. Bratt, H.J. Swanger, G.W. Beall and F.K. Dashiell (1993): Knowledge-based interpretation of seismic data in the Intelligent Monitoring System, *Bull. Seism. Soc. Am.*, in press.

Bratt, S.R. and T.C. Bache (1988): Locating events with a sparse network of regional arrays, *Bull. Seism. Soc. Am.*, 78, 780-798.

Kushnir, A.F., V.M. Lapshin, V.I. Pinsky and J. Fyen (1990): Statistically optimal event detection using small array data, *Bull. Seism. Soc. Am.*, 80 Part B, 1934-1950

Kværna, T. and F. Ringdal (1986): Stability of various F-k estimation techniques, in *NORSAR Semiannual Tech. Summ., 1-86/87*, Kjeller, Norway, 29-40.

Kværna, T. and D.J. Doornbos (1986): An integrated approach to slowness analysis with arrays and three-component stations, in *NORSAR Semiannual Tech. Summ., 1-86/87,* NORSAR, Kjeller, 41-50.

Mykkeltveit, S. and H. Bungum (1984): Processing of regional seismic events using data from small-aperture seismic arrays, *Bull. Seism. Soc. Am.,* 74, 2313-2333.

Mykkeltveit, S. (1992): Mining explosions in the Khibiny Massif (Kola Peninsula of Russia) recorded at the Apatity three-component station, Report PL-TR-92-2253, Phillips Laboratory, Hanscom Air Force Base, MA, USA.

Pisarenko, V.F., A.F. Kushnir and I.V.Savin (1987): Statistical adaptive algorithms for estimation of onset moments of seismic phases: *Phys. Earth Planet. Int.*, 47, 4-10.

Sereno, T.J. (1990): Attenuation of regional phases in Fennoscandia and estimates of arrival time and azimuth uncertainty using data recorded by regional arrays, *Semiann. Tech. Rep. No. 3, 1 Jan 89 - 30 Jun 90,* Science Applications International Corp., San Diego, CA, USA.

Mine	Location	
I, Underground	67.6702°N	33.7285°E
I, Open-pit	67.665°N	33.744°E
II	67.647°N	33.761°E
III	67.631°N	33.835°E
IV	67.624°N	33.896°E
V	67.632°N	34.011°E
VI	67.665°N	34.146°E

Table 7.2.1. The table gives the location of the six mines in the Khibiny Massif shown in Fig. 7.2.1.

Event	Mine	ESTON1 P-arrival (APA0)	Size
1	I (U)	1992-312:06.31.49.425	185 tons
2	I (U)	1992-355:07.10.51.931	190 tons
3	I (O)	1992-366:04.35.22.825	14 tons
4	I (O)	1993-017:06.51.15.831	4 tons
5	I (U)	1993-031:04.14.11.263	140 tons
6	I (O)	1993-038:07.13.16.881	7 tons
7	I (U)	1993-045:07.39.45.200	185 tons, double
8	I (O)	1993-052:07.24.49.706	14 tons, double
9	I (O)	1993-059:04.24.01.850	30 tons
10	I (O)	1993-066:06.58.54.356	12 tons
11	I (O)	1993-073:11.28.09.731	10 tons
12	I (O)	1993-080:11.26.36.106	10 tons
13	II	1992-334:04.08.51.725	130 tons
14	II	1992-366:09.41.50.156	100 tons
15	II	1993-024:08.04.48.656	24 tons
16	II	1993-066:04.14.37.475	60 tons
17	III	1992-354:08.38.32.806	15 tons
18	III	1992-361:09.53.07.550	320 tons
19	III	1993-016:09.20.47.756	20 tons
20	III	1993-030:10.16.00.581	20 tons
21	III	1993-030:13.07.15.650	265 tons
22	III	1993-044:12.05.41.725	300 tons
23	III	1993-051:07.28.29.931	16 tons
24	III	1993-058:12.01.17.356	17 tons
25	III	1993-065:08.51.42.356	18 tons
26	III	1993-065:11.00.36.931	130 tons

Event	Mine	ESTON1 P-arrival (APA0)	Size
27	II	1993-065:11.29.46.150	Induced earth-quake, M_L 2.3
28	III	1993-086:10.35.05.925	14 tons
29	IV	1992-353:12.29.32.681	340 tons
30	IV	1992-360:12.37.40.556	380 tons
31	IV	1992-365:11.39.53.300	214 tons
32	IV	1993-006:11.01.24.331	310 tons
33	IV	1993-012:12.04.00.406	130 tons
34	IV	1993-022:12.50.56.806	310 tons
35	IV	1993-036:12.35.08.831	230 tons
36	IV	1993-043:13.37.27.181	350 tons
37	IV	1993-057:12.31.59.475	380 tons
38	IV	1993-064:12.32.40.931	300 tons, double
39	IV	1993-075:12.29.49.650	70 tons
40	IV	1993-082:15.08.34.250	95 tons
41	IV	1993-089:14.44.12.256	100 tons
42	V	1992-346:08.56.58.906	183 tons
43	V	1992-360:08.03.37.581	138 tons
44	V	1993-006:08.18.41.606	101 tons
45	V	1993-015:14.08.51.075	188 tons
46	V	1993-029:10.07.17.831	195 tons
47	V	1993-036:08.05.42.006	unknown size
48	V	1993-050:12.34.53.506	203 tons
49	V	1993-057:10.33.31.006	149 tons
50	V	1993-078:09.45.13.906	260 tons, general
51	V	1993-085:08.59.22.900	146 tons
52	VI	1992-318:06.41.16.250	60 tons
53	VI	1992-332:07.05.26.950	unknown size

Event	Mine	ESTON1 P-arrival (APA0)	Size
54	VI	1992-353:07.35.26.956	73 tons
55	VI	1992-365:07.23.22.631	80 tons
56	VI	1993-022:08.20.09.231	285 tons
57	VI	1993-043:08.13.29.381	140 tons
58	VI	1993-071:07.33.22.906	140 tons, general

Table 7.2.2. This table contains information on the 58 Khibiny Massif events analyzed in this study. For each event, the assigned mine, the automatic P-onset at the Apatity array and the event size are given. I(U) means the underground Mine I, whereas I(O) means the open-pit mine. When the event size is given as "double", the reported charge is distributed between two explosions that are closely separated in time. If the term "general" is used, the reported charge is distributed among several explosions that are closely separated in time.

Mine	APA0		APZ9		ARCESS	
	Delta (km)	Az (deg)	Delta (km)	Az (deg)	Delta (km)	Az (deg)
I(U)	32.0	76.8	17.8	50.4	393.8	118.0
I (O)	32.6	78.0	18.0	53.1	394.7	118.0
II	33.0	81.7	17.5	59.8	396.4	118.2
III	35.9	85.2	19.6	69.0	400.0	118.1
IV	38.4	86.6	21.8	73.3	402.6	118.0
V	43.4	85.7	26.7	74.4	406.0	117.5
VI	49.4	81.8	33.3	70.8	408.6	116.6

Table 7.2.3. Distance and azimuths from the three stations APA0, APZ9 and ARCESS to the mines considered in this study.

	σ_{manual}	$\sigma_{automatic}$
P, Apatity array	0.04 s	0.04 s
P, Apatity 3-comp.	0.06 s	0.05 s
Pn, ARCESS	0.06 s	0.05 s

Table 7.2.4. Estimated standard deviations of manual and automatic (ESTON1) P-onsets at the Apatity array, the Apatity three-component station and at ARCESS.

S-phase	Reference phase	σ_{manual}	$\sigma_{automatic}$
APA0	P at APA0	0.20	0.19
	P at APZ9	0.20	0.19
	Pn at ARCESS	0.18	0.20
APA0	Average	0.19	0.19
APZ9	P at APA0	0.13	0.15
	P at APZ9	0.12	0.14
	Pn at ARCESS	0.13	0.16
APZ9	Average	0.13	0.15

Table 7.2.5. Estimated standard deviations of manual and automatic (ESTON3) S-onsets at APA0 and APZ9. In addition to the average uncertainty, we give for each phase the uncertainty estimates computed using the three different reference phases.

	Mean (^{0})	σ (^{0})
P, Apatity array	8.2	3.9
Pn, ARCESS	4.6	0.9
S, Apatity array	-1.0	19.8
Rg, Apatity array	-1.8	3.4

Table 7.2.6. Mean and standard deviation of azimuth residuals relative to Khibiny mine locations.

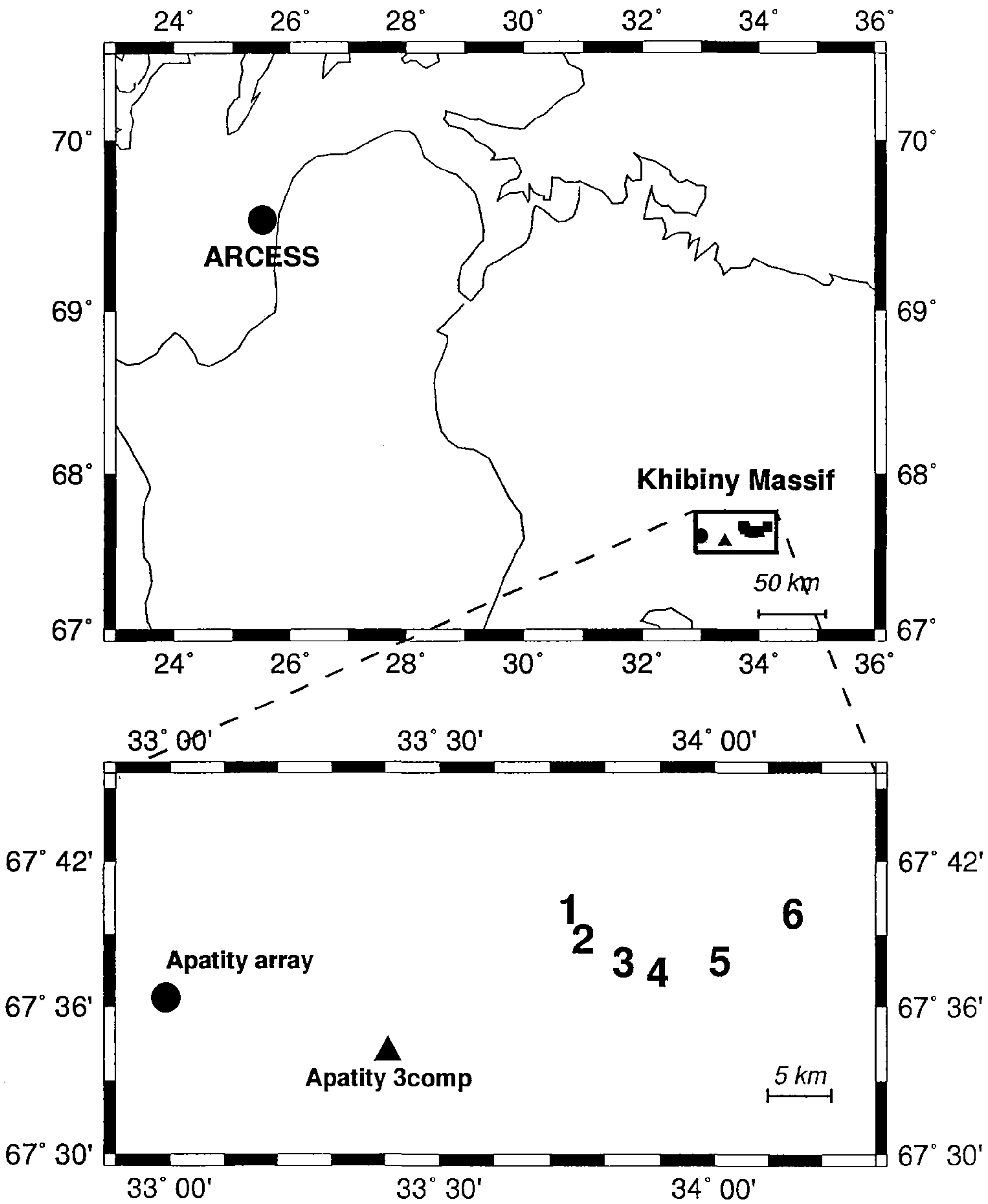

Fig. 7.2.1. In the **upper part** , a large reference area is shown. The location of the ARCESS array is given by a filled circle, and the location of the Khibiny Massif region is shown. The **lower part** shows a detailed picture of the Khibiny Massif region. The locations of the six mining sites are given by large numbers 1-6. The Apatity array is shown as a filled circle and the three-component station in the town of Apatity is shown as a large triangle.

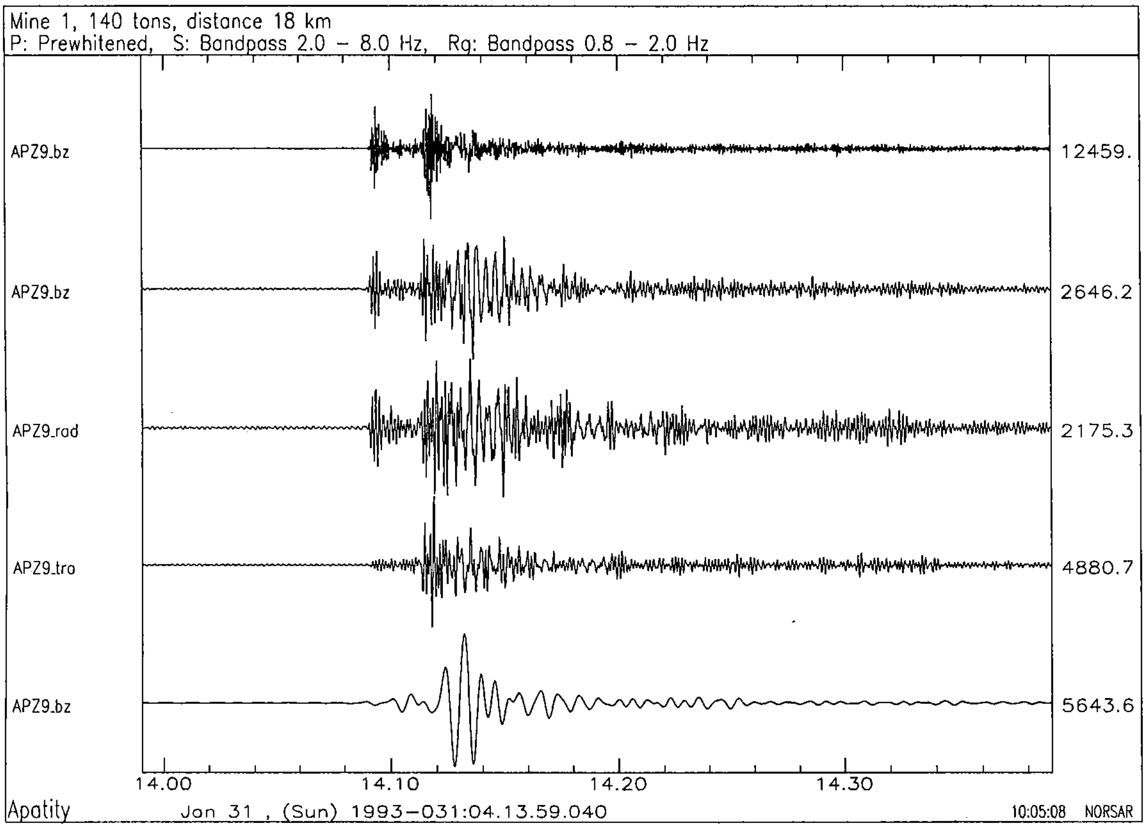

Fig. 7.2.2. Seismograms from an event at the underground Mine I recorded at the Apatity three-component station. The source-receiver distance is 18 km. The upper trace, emphasizing the P-phase, is the z-component prewhitened with a low-order prediction error filter designed from a 25 s noise sample preceding the P-phase. The three-component data rotated with the azimuth to the mine can be seen at traces 2-4. The data are filtered in a relatively wide passband of 2 - 8 Hz, and these three traces clearly show an instantaneous S-phase. The lower trace is bandpass filtered between 0.8 and 2.0 Hz, and clearly illustrate the low-frequency Rg phase.

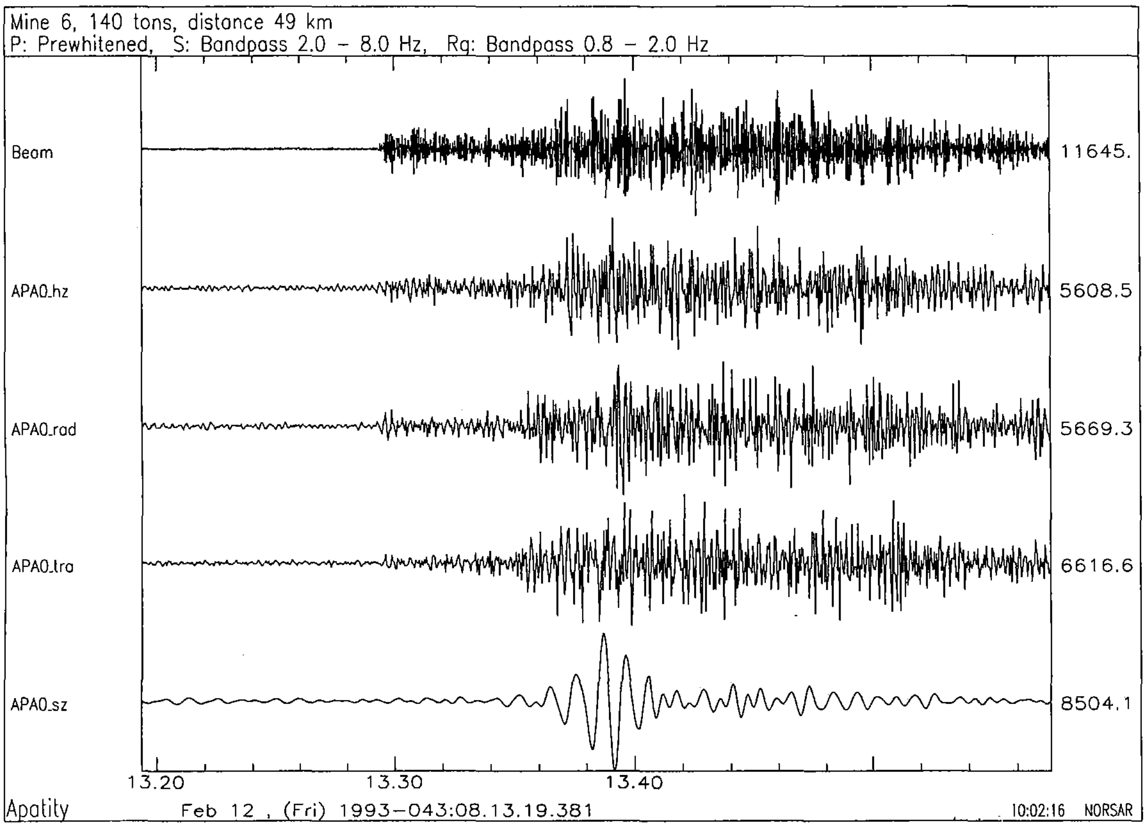

Fig. 7.2.3. Seismograms from an event at mine VI recorded at the Apatity array. The source-receiver distance is 49 km. The only difference from the traces of Fig. 7.2.2 is that the upper trace is the array beam steered with steering delays corresponding to the slowness and azimuth of the P-arrival. Notice that in this case the S-phase is much more emergent than the S-phase of Fig. 7.2.2.

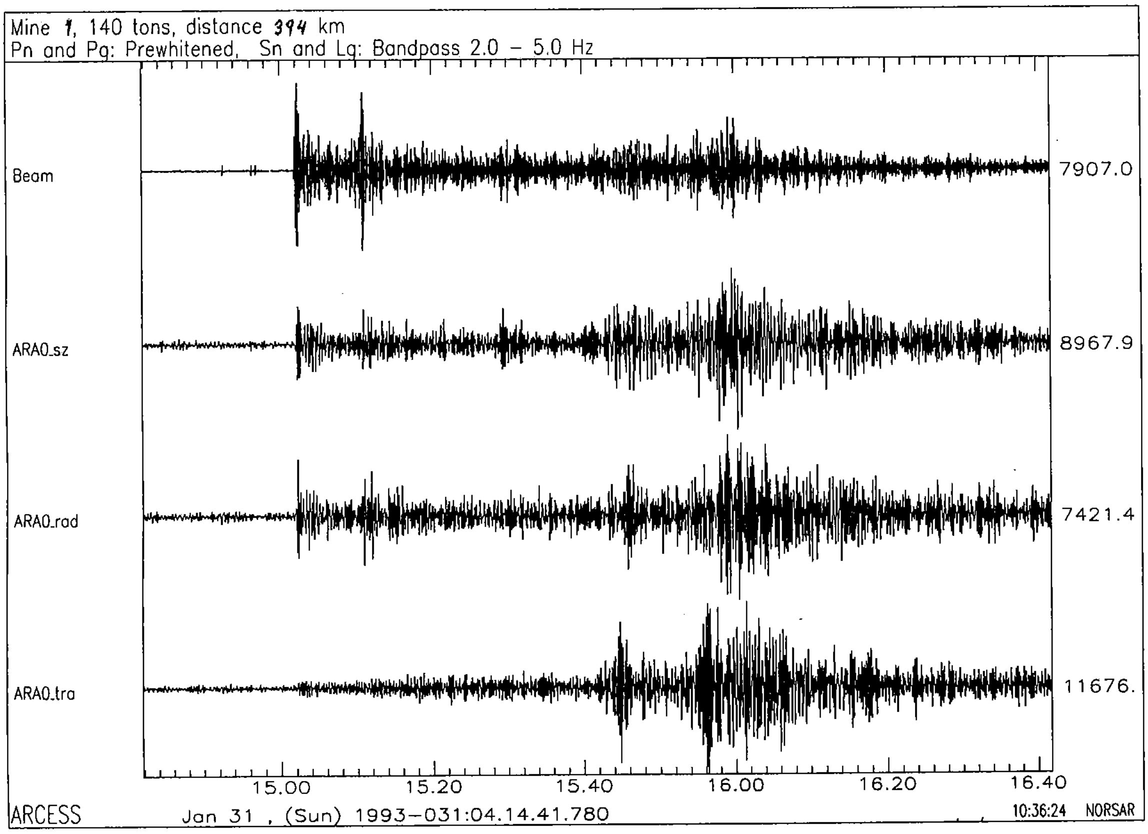

Fig. 7.2.4. ARCESS recording of the event also shown in Fig. 7.2.2. The source-receiver distance is 394 km. The upper trace is the array beam steered with the slowness and azimuth of the P-phase. The beam is prewhitened with a low-order prediction error filter. The lower three traces are the rotated three-component data at the central element (ARA0) of the ARCESS array. The data are bandpass filtered between 2 and 5 Hz. Notice that both Pn, Pg, Sn and Lg are clearly seen, and that Sn and Lg are most prominent on the transverse component.

a)

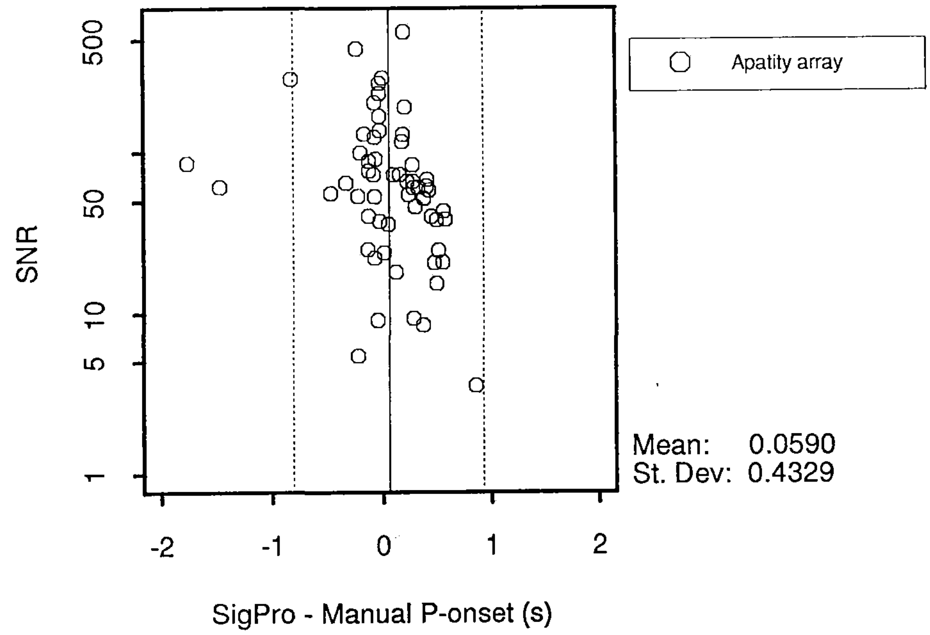

b)

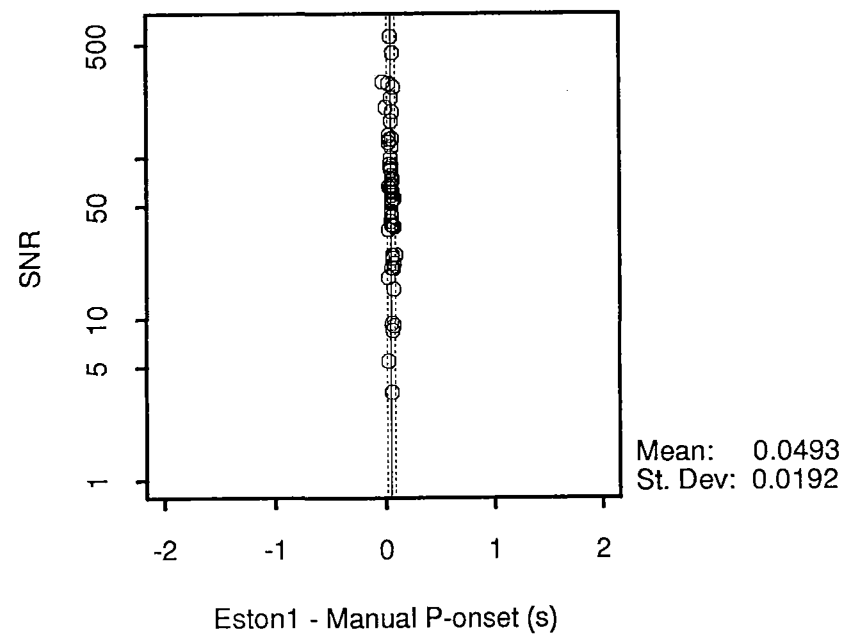

Fig. 7.2.5. These two plots show the time differences between the automatic P-onsets and the manual pick at APA0 as a function of signal-to-noise ratio (SNR) on the prewhitened beam. All 58 P-observations are included. Figure **a)** shows the time differences between the automatic P-onsets from the IMS and the manual picks, whereas figure **b)** shows the time differences between the automatic P-onsets from ESTON1 and the manual picks. The two vertical dotted lines represent $\pm\sigma 2$.

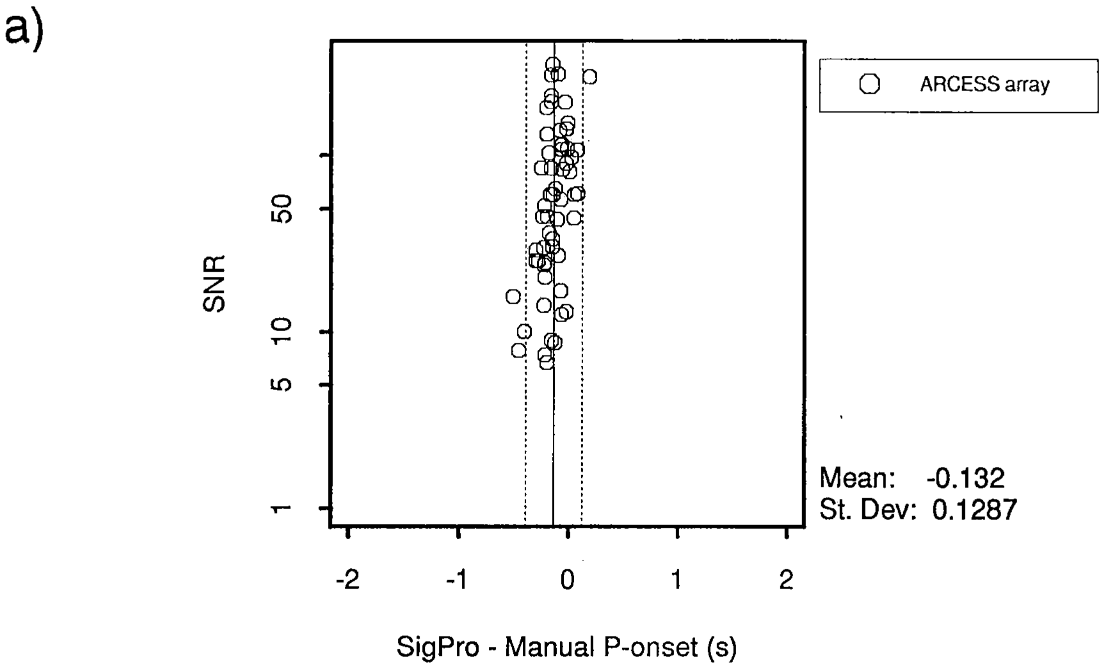

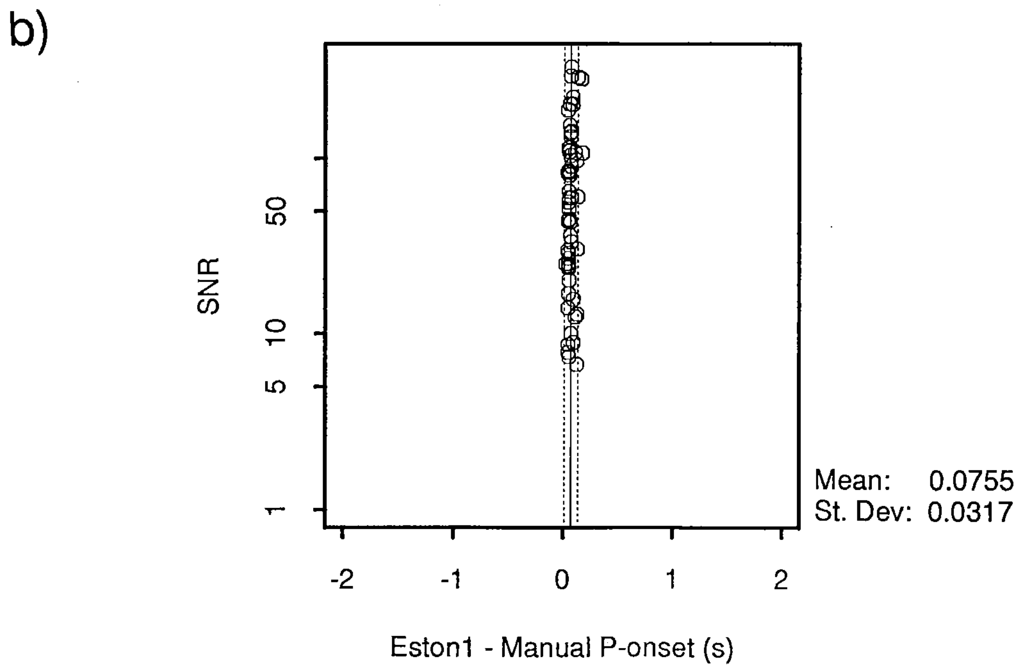

Fig. 7.2.6. Plots similar to those of Fig. 7.2.5, but in this case for Pn-onsets at ARCESS. For one of the Khibiny Massif events, the ARCESS array was not operational, and consequently only 57 P-phases were analyzed.

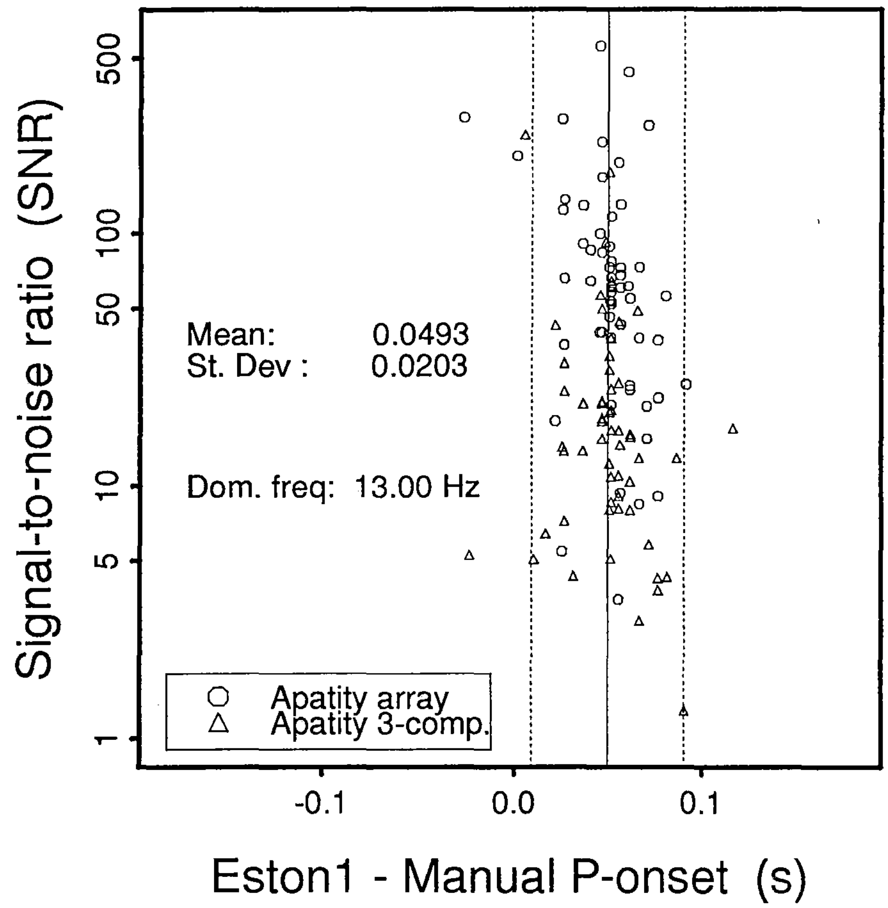

Fig. 7.2.7. This figure show the time differences between the automatic P-onsets from ESTON1 and the manual pick at both Apatity stations (APA0 and APZ9) as a function of signal-to-noise ratio (SNR). Compared to Fig. 7.2.5 the x-axis is strongly expanded. Notice that P-phases at APZ9 (triangles) generally have lower SNR. The average dominant frequency of these P-phases is 13 Hz.

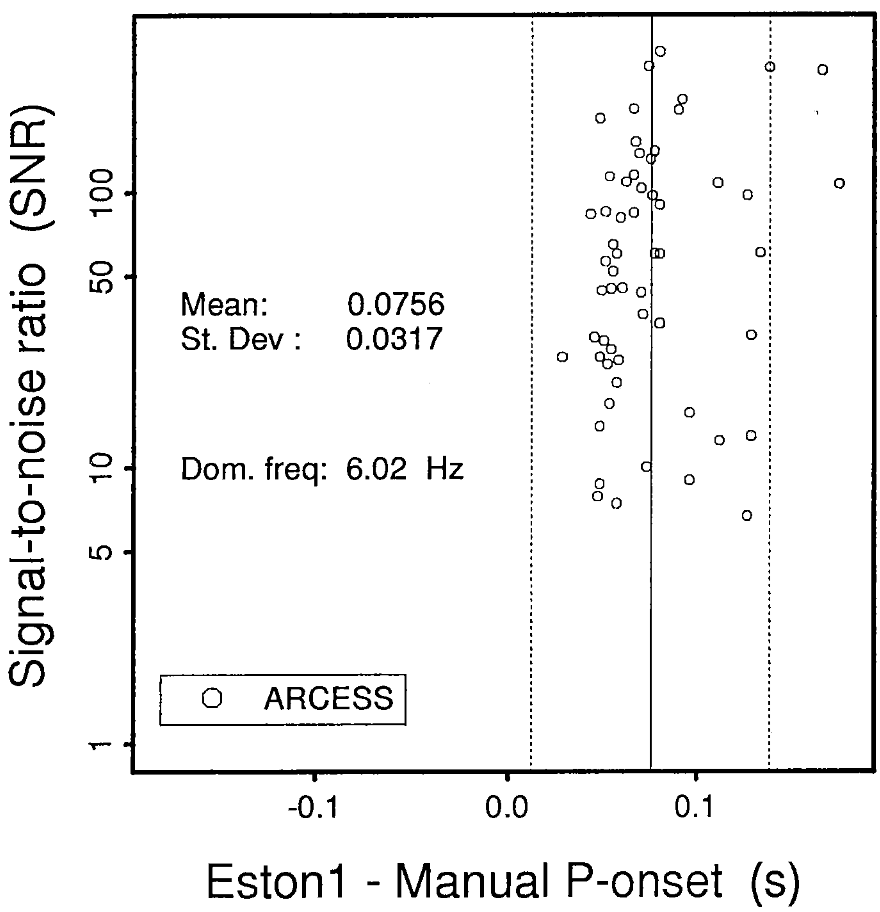

Fig. 7.2.8. Plot similar to Fig. 7.2.7, but in this case for ARCESS P. The average dominant frequency is 6 Hz.

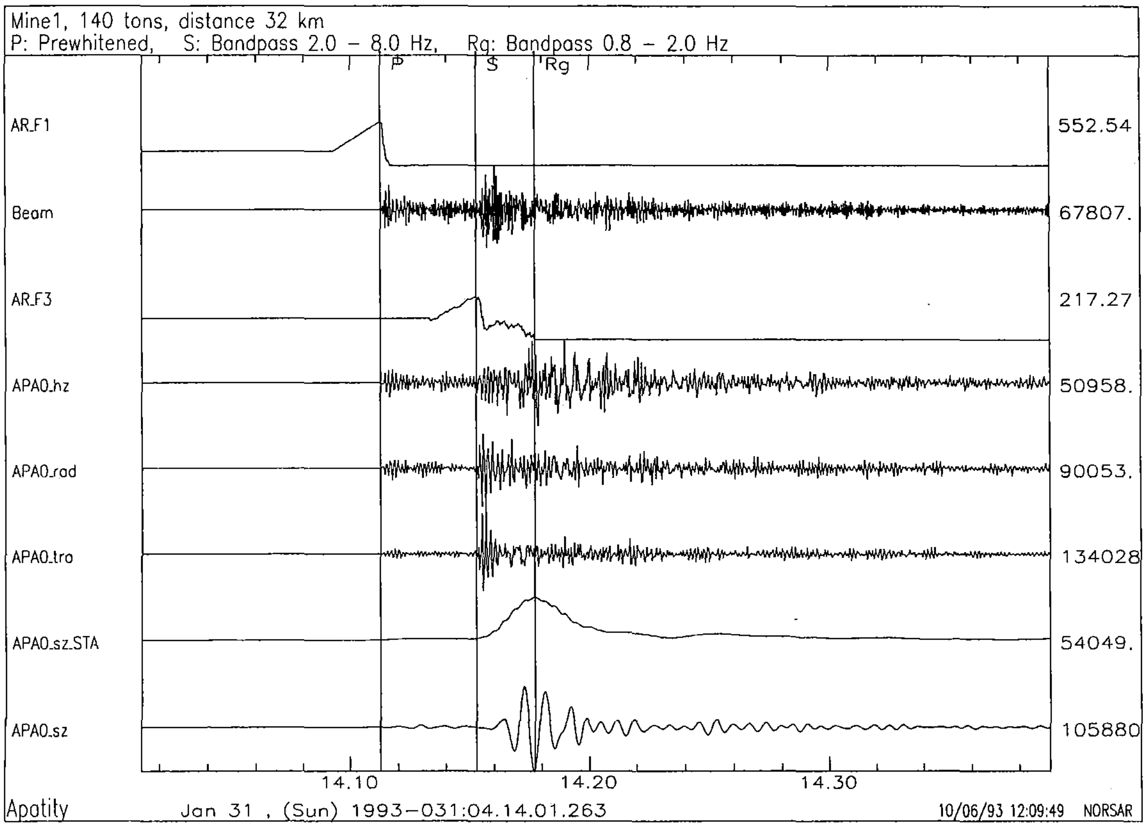

Fig. 7.2.9. The seismograms of this figure are Apatity array (APA0) recordings of the Mine I event also given in Fig. 7.2.2. The source-receiver distance is 32 km. Trace no. 2 is the prewhitened P-beam used for onset-time estimation using ESTON1. The upper trace gives the likelihood function from ESTON1 after processing an interval of ±2 s around the initial P-onset estimate, and the peak of this likelihood function correspond to the estimated onset. The lower trace is the vertical component APA0_sz filtered in a low passband (0.8 - 2.0 Hz) to enhance the Rg phase, and the trace above it is the STA envelope. The peak of this envelope is defined as the peak of the Rg phase. After the P-onset and the Rg maximum is found, we are searching for the S-onset using the three-component ESTON3 estimator. The search interval starts 2 s after the P-onset and stops at the Rg peak, as seen from the ESTON3 likelihood function of trace no. 3. The three-component data processed by ESTON3 are given in traces 4-7. Notice that there is no need to rotate the three-component data before using ESTON3, but to visualize that the S-phase has the largest SNR on the transverse component, we have in this figure rotated the data. Notice that both the ESTON1 and the ESTON3 likelihood functions show clear peaks at the P- and S-onsets.

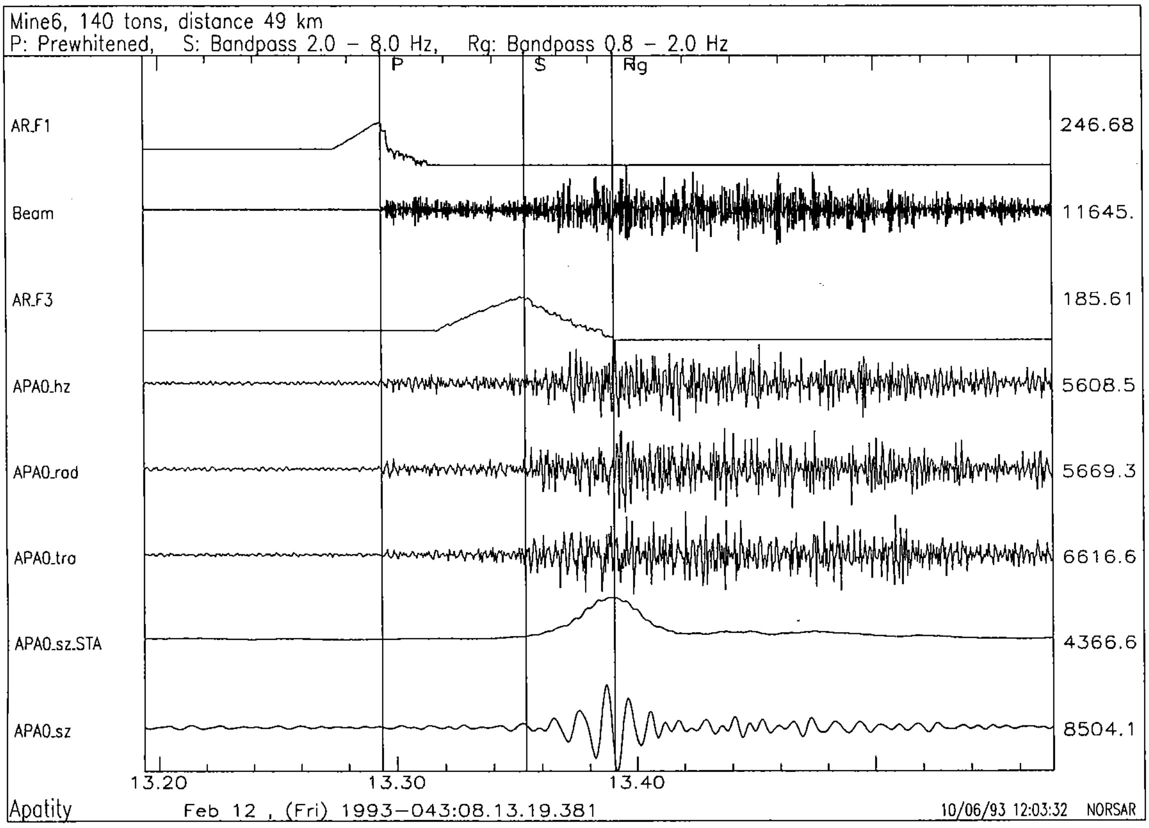

Fig. 7.2.10. The traces of this plot are similar to those of Fig. 7.2.9. The seismograms are Apatity array (APA0) recordings of the Mine VI event also shown in Fig. 7.2.3. The source-receiver distance is 49 km. Notice that the S-phase is much more emergent than the S-phase of Fig. 7.2.9, but the ESTON3 likelihood function still shows a clear peak at the S-onset.